Bull. Mater. Sci., Vol. 32, No. 2, April 2009, pp. 149–153. © Indian Academy of Sciences.

Synthesis and characterization of nano-sized $Ba_xSr_{1-x}SO_4$ ($0 \le x \le 1$) solid solution by a simple surfactant-free aqueous solution route

YU-FENG LI, JIA-HU OUYANG*, YU ZHOU, XUE-SONG LIANG and JI-YONG ZHONG
Institute for Advanced Ceramics, Department of Materials Science, Harbin Institute of Technology, PO Box 433, Harbin 150001, PR China

MS received 1 July 2008

Abstract. **A facile aqueous solution route has been employed to synthesize $Ba_xSr_{1-x}SO_4$ ($0 \le x \le 1$) solid solution nanocrystals at room temperature without using any surfactants or templates. The as-synthesized products were characterized by means of X-ray diffraction (XRD), X-ray fluorescence spectrometer (XRF), scanning electron microscopy (SEM), and differential scanning calorimetry–thermogravimetry (DSC–TG). The $Ba_xSr_{1-x}SO_4$ solid solution nanocrystals exhibit an orthorhombic structure and an ellipsoidal-shaped morphology with an average size of 80–100 nm. The lattice parameters of $Ba_xSr_{1-x}SO_4$ solid solution crystals increase with increasing x value. However, they are not strictly coincident with the Vegard's law, which indicates that the as-obtained products are non-ideal solid solutions. The $Ba_xSr_{1-x}SO_4$ solid solution nanocrystals have an excellent thermal stability from ambient temperature to 1300°C with a structural transition from orthorhombic to cubic phase at about 1111°C.**

Keywords. **$Ba_xSr_{1-x}SO_4$ ($0 \le x \le 1$) solid solution; nanomaterials; structural transition; aqueous solution route; surfactant-free.**

1. Introduction

In recent years, nanoscale materials with special size and controlled morphology have generated important scientific interest due to their excellent physical and chemical properties and potential applications (Xia *et al* 2003; Li *et al* 2005; Whitesides 2005). Because of this, various and effective approaches have been explored to obtain the nanomaterials, such as physical and chemical vapour deposition methods (Granqvist and Buhrman 1976; Hitchman and Jensen 1993), sol–gel processes (Sanchez and Ribot 1994; Shek *et al* 1999), mechanochemical synthesis routes (Baburaj *et al* 1997; Dodd *et al* 2001) and so on. However, it is still an important challenge to obtain large quantities of nanoparticles by simple and powerful methods. Nowadays, the solution-phase methods have been considered as one of the most promising routes for the synthesis of nanocrystals with some significant advantages, including less-complicated techniques, low-cost and large-scale production (Cheng *et al* 2004; Yuan *et al* 2005; Zhu *et al* 2007; Li *et al* 2008).

Both barium sulfate (barite) and strontium sulfate (celestite) are important inorganic chemical products, and have been widely used as significant industrial raw materials in ceramics, pigments, cosmetics, papermaking, electronics and high temperature solid lubricants and so on. Barite and celestite as well as the family members of $Ba_xSr_{1-x}SO_4$ solid solution can form from seawater as authigenic minerals or as a result of hydrothermal process (Feely *et al* 1987). In recent years, study on synthesis of $BaSO_4$, $SrSO_4$ and their solid solutions has received considerable attention for the interest of mineralogical, industrial and environmental aspects (Putniss *et al* 1992). However, characterization and structural transition of $Ba_xSr_{1-x}SO_4$ solid solutions were not reported yet in the open literatures. In the present paper, $Ba_xSr_{1-x}SO_4$ ($0 \le x \le 1$) solid solution nanocrystals were fabricated for the first time through a facile aqueous solution method at room temperature without adding any surfactants or organic additives. The structure and thermal stability of the as-obtained $Ba_xSr_{1-x}SO_4$ solid solution nanocrystals were studied.

2. Experimental

Analytically pure $BaCl_2{\cdot}2H_2O$, $SrCl_2{\cdot}6H_2O$, Na_2SO_4 and ethanol were used as the starting materials without further purification. In this investigation deionized water was used. In a typical synthesis, 66 mL ethanol was added into a 100 mL solution of $BaCl_2$ and $SrCl_2$ under stirring to form a homogeneous aqueous solution. Then, a 120 mL Na_2SO_4 solution was added quickly into the mixed aqueous solution of $BaCl_2$, $SrCl_2$ and ethanol under vigorous stirring to produce white precipitates at

*Author for correspondence (ouyangjh@hit.edu.cn)

Table 1. Various initial concentrations of $BaCl_2$, $SrCl_2$ and Na_2SO_4 in selected solutions denoted by different x values from 0 to 1.

Sample	$BaCl_2$ (mol/L)	$SrCl_2$ (mol/L)	Na_2SO_4 (mol/L)
x = 0 ($SrSO_4$)	0	1·0	1·0
x = 0·25 ($Ba_{0.25}Sr_{0.75}SO_4$)	0·25	0·75	1·0
x = 0·5 ($Ba_{0.5}Sr_{0.5}SO_4$)	0·5	0·5	1·0
x = 0·75 ($Ba_{0.75}Sr_{0.25}SO_4$)	0·75	0·25	1·0
x = 1 ($BaSO_4$)	1·0	0	1·0

Table 2. The mass percentages (wt.%) of barium and strontium in $Ba_xSr_{1-x}SO_4$ solid solution products with various x values of 0·25–0·75.

	Theoretical results (wt.%)		Experimental results (wt.%)	
Sample	Barium	Strontium	Barium	Strontium
x = 0·25 ($Ba_{0.25}Sr_{0.75}SO_4$)	17·5	33·5	17·1	33·4
x = 0·5 ($Ba_{0.5}Sr_{0.5}SO_4$)	32·9	21·0	32·7	20·5
x = 0·75 ($Ba_{0.75}Sr_{0.25}SO_4$)	46·6	9·9	46·3	9·7

Table 3. Calculated lattice parameters a, b and c of $Ba_xSr_{1-x}SO_4$ solid solution crystals with various x values from 0–1 according to the XRD data of characteristic peaks.

	Lattice parameters (Å)		
Sample	a	b	c
x = 0 ($SrSO_4$)	6·866	8·359	5·352
x = 0·25 ($Ba_{0.25}Sr_{0.75}SO_4$)	6·936	8·477	5·395
x = 0·5 ($Ba_{0.5}Sr_{0.5}SO_4$)	7·006	8·604	5·421
x = 0·75 ($Ba_{0.75}Sr_{0.25}SO_4$)	7·079	8·733	5·442
x = 1 ($BaSO_4$)	7·157	8·881	5·454

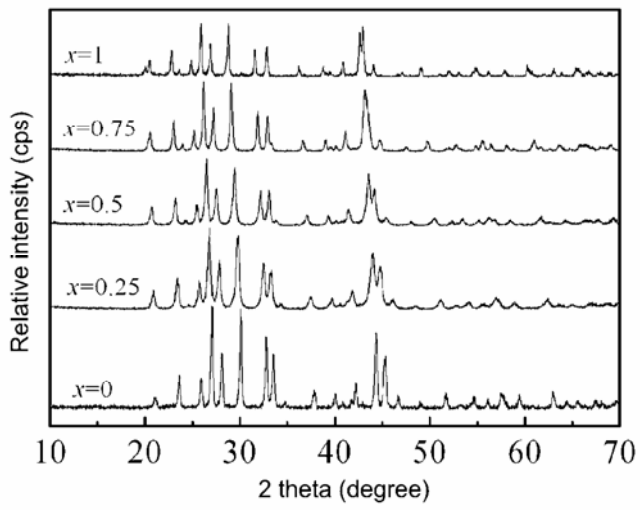

Figure 1. X-ray diffraction patterns of $Ba_xSr_{1-x}SO_4$ solid solution particles with various x values from 0 to 1. (a) x = 0 ($SrSO_4$); (b) x = 0·25 ($Ba_{0.25}Sr_{0.75}SO_4$); (c) x = 0·5 ($Ba_{0.5}Sr_{0.5}SO_4$); (d) x = 0·75 ($Ba_{0.75}Sr_{0.25}SO_4$) and (e) x = 1 ($BaSO_4$).

room temperature. Various initial concentrations of $BaCl_2$, $SrCl_2$ and Na_2SO_4 in selected solutions denoted by different x values from 0–1 are shown in table 1. After continuous stirring for 10 min, the suspension was kept under static conditions for 24 h. The $Ba_xSr_{1-x}SO_4$ solid solution precipitates were then filtered off and rinsed several times by water and ethanol, respectively. Finally, $Ba_xSr_{1-x}SO_4$ solid solution particles were obtained after drying at 80°C for 12 h.

The phase structure of $Ba_xSr_{1-x}SO_4$ solid solution products was identified by X-ray diffraction (XRD; Rigaku D/Max 2200VPC) using Cu$K\alpha$ radiation at a scan rate of 4° min^{-1} in a 2θ range of 10–70°. The mass percentages (wt.%) of barium and strontium in the as-obtained $Ba_xSr_{1-x}SO_4$ solid solution precipitates were determined by an X-ray fluorescence spectrometer (PANalytical AXIOS PW4400). The morphology and size of $Ba_xSr_{1-x}SO_4$ solid solution particles were examined by means of a scanning electron microscopy (SEM; Camscan MX-2600FE) using an accelerating voltage of 20 kV. The differential scanning

calorimetry–thermogravimetry (DSC–TG) analysis was performed using a TG–DSC instrument (NETZSCH STA449C) at an air flow rate of 30 ml min^{-1} and a heating rate of 10°C min^{-1} from room temperature to 1300°C.

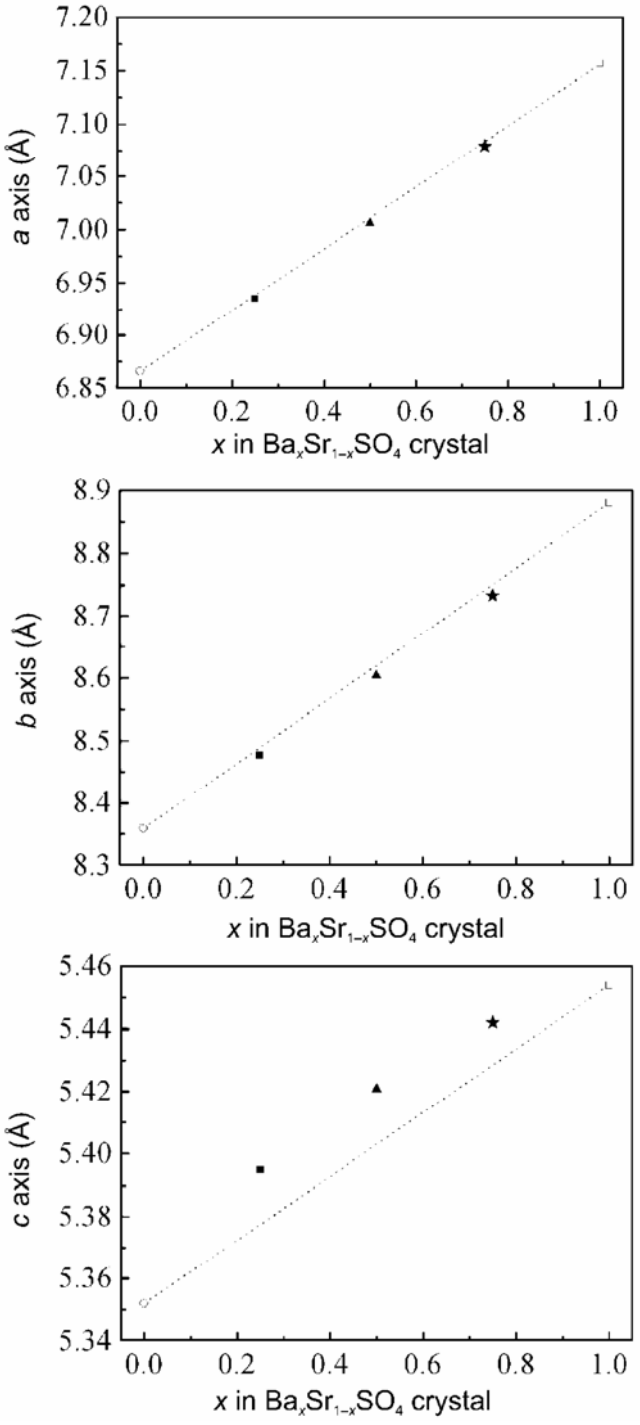

Figure 2. Lattice parameters *a*, *b* and *c* of $Ba_xSr_{1-x}SO_4$ solid solution crystals as a function of *x* value from 0 to 1: (○) $x = 0$ ($SrSO_4$), (■) $x = 0{\cdot}25$ ($Ba_{0{\cdot}25}Sr_{0{\cdot}75}SO_4$); (▲) $x = 0{\cdot}5$ ($Ba_{0{\cdot}5}Sr_{0{\cdot}5}SO_4$); (✶) $x = 0{\cdot}75$ ($Ba_{0{\cdot}75}Sr_{0{\cdot}25}SO_4$) and (□) $x = 1$ ($BaSO_4$).

3. Results and discussion

Figure 1 shows X-ray diffraction patterns of $Ba_xSr_{1-x}SO_4$ solid solution particles with various *x* values from 0 to 1.

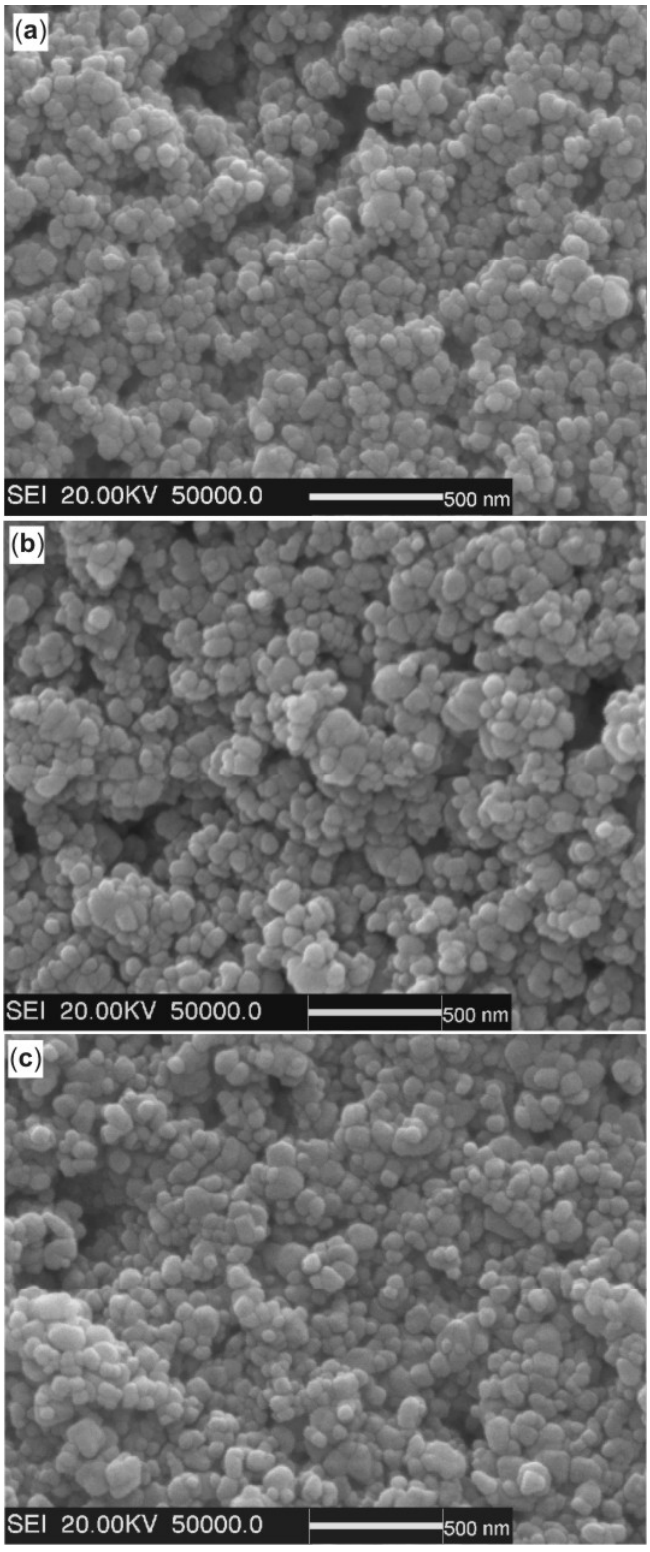

Figure 3. Typical SEM images of $Ba_xSr_{1-x}SO_4$ solid solution nanocrystals with various *x* values from 0·25–0·75: (**a**) $x = 0{\cdot}25$ ($Ba_{0{\cdot}25}Sr_{0{\cdot}75}SO_4$); (**b**) $x = 0{\cdot}5$ ($Ba_{0{\cdot}5}Sr_{0{\cdot}5}SO_4$) and (**c**) $x = 0{\cdot}75$ ($Ba_{0{\cdot}75}Sr_{0{\cdot}25}SO_4$).

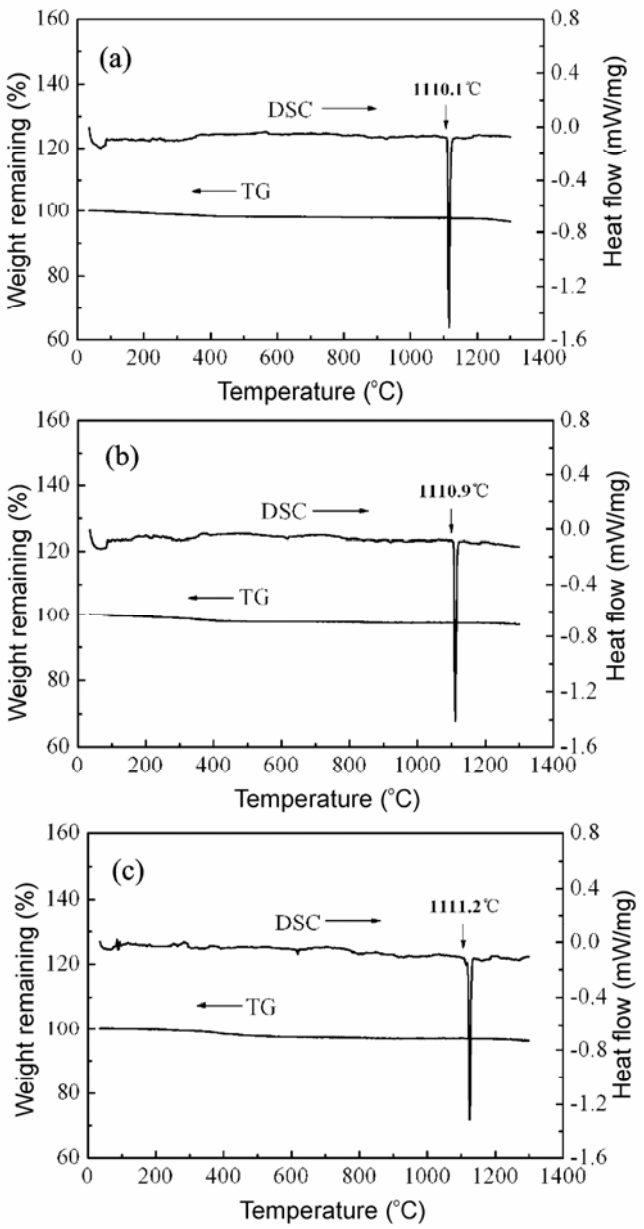

Figure 4. TG/DSC thermal analysis curves of $Ba_xSr_{1-x}SO_4$ solid solution nanocrystals with various x values of 0·25, 0·5 and 0·75: (**a**) $x = 0{\cdot}25$ ($Ba_{0{\cdot}25}Sr_{0{\cdot}75}SO_4$); (**b**) $x = 0{\cdot}5$ ($Ba_{0{\cdot}5}Sr_{0{\cdot}5}SO_4$) and (**c**) $x = 0{\cdot}75$ ($Ba_{0{\cdot}75}Sr_{0{\cdot}25}SO_4$).

Clearly, the $Ba_xSr_{1-x}SO_4$ solid solution products are well crystallized from strong and sharp diffraction peaks in the XRD patterns. All the diffraction peaks of different $Ba_xSr_{1-x}SO_4$ samples are perfectly indexed as a single phase of orthorhombic with a space group, *Pbnm*(62) of $SrSO_4$ (JCPDS Card 05-0593), $Ba_{0{\cdot}25}Sr_{0{\cdot}75}SO_4$ (JCPDS Card 39-1467), $Ba_{0{\cdot}5}Sr_{0{\cdot}5}SO_4$ (JCPDS Card 39-1468), $Ba_{0{\cdot}75}Sr_{0{\cdot}25}SO_4$ (JCPDS Card 39-1469), and $BaSO_4$ (JCPDS Card 24-1035), respectively. As impurity phases were not detected in XRD patterns, the $Ba_xSr_{1-x}SO_4$ solid solution particles are considered to have a high purity.

The mass percentages (wt.%) of barium and strontium in $Ba_xSr_{1-x}SO_4$ solid solution products with various x values of 0·25–0·75 were given in table 2 by using an X-ray fluorescence spectrometer. For a comparative study, theoretical calculation data were also listed in table 2. It can be seen that the experimental results on the mass percentages of barium and strontium in $Ba_xSr_{1-x}SO_4$ solid solution products are closely approaching the theoretical calculation data, which are also in good agreement with XRD analysis. It demonstrates that all the barium and strontium ions in these solutions almost precipitate to completion. According to the XRD data of characteristic peaks, the lattice parameters a, b and c of $Ba_xSr_{1-x}SO_4$ solid solution crystals with various x values from 0 to 1 were calculated as shown in table 3. The lattice parameters a, b and c as a function of x value are illustrated in figure 2. Clearly, there are negative deviations for the axes of a and b and a positive deviation for the c axis. This is not strictly coincident with the Vegard′s law, and indicates that the obtained $Ba_xSr_{1-x}SO_4$ products are non-ideal solid solutions (West 1984).

Typical SEM images of $Ba_xSr_{1-x}SO_4$ solid solution products with various x values from 0·25–0·75 are shown in figure 3. The $Ba_xSr_{1-x}SO_4$ solid solution products contain a large quantity of ellipsoidal-shaped nanocrystals with an average size of 80–100 nm. Moreover, these $Ba_xSr_{1-x}SO_4$ nanocrystals with various x values from 0·25–1 exhibit a similar size and morphology.

Figure 4 shows the TG/DSC thermal analysis curves of $Ba_xSr_{1-x}SO_4$ solid solution nanocrystals with various x values of 0·25, 0·5 and 0·75 from room temperature to 1300°C. There is almost no weight loss from ambient temperature to 1300°C, indicating that the $Ba_xSr_{1-x}SO_4$ solid solution nanocrystals have an excellent thermal stability over a broad temperature range. From the DSC curves in figure 4, the endothermic peak at 1110·1°C, 1110·9°C and 1111·2°C are found for $Ba_xSr_{1-x}SO_4$ solid solution nanocrystals with various x values of 0·25, 0·5 and 0·75, respectively. The presence of endothermic peak is attributed to a structural transition of $Ba_xSr_{1-x}SO_4$ solid solution crystal from orthorhombic to cubic phases, and the structural transition temperature are slightly lower than those of pure $BaSO_4$ (1149°C) and $SrSO_4$ (1140°C) crystals (Torres *et al* 1999).

4. Conclusions

In summary, $Ba_xSr_{1-x}SO_4$ ($0 \le x \le 1$) solid solution nanocrystals were successfully fabricated with a simple surfactant-free aqueous solution method. The $Ba_xSr_{1-x}SO_4$ solid solution nanocrystals exhibit an orthorhombic structure and an ellipsoidal-shaped morphology with an average size of 80–100 nm. The lattice parameters of $Ba_xSr_{1-x}SO_4$ solid solution crystals increase with increasing x value. However, they are not strictly coincident with the

Vegard's law, which indicates that the as-obtained products are non-ideal solid solution. The $Ba_xSr_{1-x}SO_4$ solid solution nanocrystals have an excellent thermal stability from ambient temperature to 1300°C with a structural transition from orthorhombic to cubic phases at about 1111°C.

Acknowledgements

The authors would like to thank financial support from the National 863 High-Tech Project (2006AA03Z537), the National Natural Science Foundation of China (NSFC-No. 50572020), and the Program for New Century Excellent Talents in University (NCET-06-0339).

References

Baburaj E G, Hubert K T and (Sam) Froes F H 1997 *J. Alloys Compd.* **257** 146

Cheng B, Russell J M, Shi W S, Zhang L and Samulski E T 2004 *J. Am. Chem. Soc.* **126** 5972

Dodd A C, Raviprasad K and McCormick P G 2001 *Scr. Mater.* **44** 689

Feely R A, Gammon R H, Taft B A, Pullen P E, Waterman L S, Conway T J, Gendron J F and Wisegarver D P 1987 *J. Geophys. Res.* **92** 6545

Granqvist C G and Buhrman R A 1976 *J. Appl. Phys.* **47** 2200

Hitchman M L and Jensen K F 1993 *Chemical vapour deposition – principles and applications* (London: Academic Press)

Li X D, Wang X N, Xiong Q H and Eklund P C 2005 *Appl. Phys. Lett.* **87** 233113

Li Y F, Ouyang J H and Zhou Y 2008 *Mater. Chem. Phys.* **111** 508

Putniss A, Fernandez-Diaz L and Prieto M 1992 *Nature* **358** 743

Sanchez C and Ribot F 1994 *New J. Chem.* **18** 1007

Shek C H, Lai J K L and Lin G M 1999 *Nanostruct. Mater.* **11** 887

Torres J, Mendez J and Sukiennik M 1999 *Thermochim. Acta* **334** 57

West A R 1984 *Solid state chemistry and its applications* (Chichester: Wiley)

Whitesides G M 2005 *Small* **2** 172

Xia Y N *et al* 2003 *Adv. Mater.* **15** 353

Yuan J K, Li W N, Gomez S and Suib S L 2005 *J. Am. Chem. Soc.* **127** 14184

Zhu L, Meng J and Cao X Q 2007 *Eur. J. Inorg. Chem.* **24** 3863